Meteorologische Zeitschrift, PrePub DOI 10.1127/metz/2017/0812

PrePub Article

Precipitation extremes on time scales from minute to month measured at the Hamburg Weather Mast 1997–2014 and their relation to synoptic weather types

Christian Weder[1,2], Gerd Müller[1*] and Burghard Brümmer[1]

[1]Meteorological Institute, CEN, University of Hamburg, Germany
[2]F2E Fluid & Energy Engineering GmbH & Co KG, Hamburg, Germany

(Manuscript received June 20, 2016; in revised form May 22, 2017; accepted May 24, 2017)

Abstract

Precipitation amount and duration measured at the Hamburg Weather Mast with 1-minute time resolution during the 17-year period 1997–2014 are used for a statistical analysis of precipitation extremes for various aggregation times (AT) from minute to month. Extremes are defined here by the 95th, 99th percentile and the absolute maximum of the PDF and are calculated for the total 17-year period and data subsets such as same months and same hours of the day to determine annual and diurnal cycles. Mean monthly precipitation amount (duration) has a maximum in July (December) and a minimum in April (April). Monthly extremes of precipitation amount for AT = 1d, 1 h and 1 min follow the mean annual cycle only partly with their maxima also in July/August but their minima in February. Hourly extremes of precipitation amount for AT = 1 h and 1 min show no diurnal cycle in winter but a clear one in summer where the corresponding maxima all occur in the afternoon time window 14–18 CET. The 95th and 99th percentile values for the total 17-year period follow power laws over the entire AT range from 1 min to 1 month. This does not hold for the maxima; the well-known Jennings power law underestimates the maxima in the sub-daily and particularly sub-hourly AT range. Our results can be used to estimate sub-daily (-hourly) extremes for stations with e.g. only daily records.

Extreme precipitation needs favourable large-scale conditions. We test the potential of the DWD (Deutscher Wetterdienst) weather type classification as downscaling predictor of extreme precipitation. All days (hours) exceeding the 95th (99th) percentile of 13.8 mm/d (5.2 mm/h) are inspected. Daily (hourly) extremes show up in 22 (18) of the 40 weather types. While in winter one north-westerly weather type occurs outstandingly frequent, several south-westerly weather types are equally frequent in summer. However, the probability that these weather types, when they occur, lead to extreme daily (hourly) precipitation is not higher than 16 % (19 %). The higher number of weather types involved in summer than winter extremes can be attributed to the modes of precipitation (stratiform, convective) classified from the amount-duration relationship. From composites of the leading weather types for days with and without extreme precipitation and from a separate (stratiform, convective) inspection of the large-scale flow situation, we identify overarching synoptic features which occur with extreme days but are not captured by the indices of the DWD classification. The potential of the classification as downscaling predictor of extreme precipitation is limited but may be improved by some simple extensions.

Keywords: Hamburg Weather Mast, precipitation amount and duration with 1-min sampling rate, PDFs and extremes of precipitation from minute to month, annual and diurnal cycle of extremes, objective weather type classification, downscaling of precipitation extremes

1 Introduction

Rain formation is a complex process which involves many scales ranging from the cloud microphysics scale to the large synoptic scale. The quantitative forecast of precipitation and particularly extreme precipitation is still difficult (e.g. Dierer et al., 2009; Sukovich et al., 2014; Bauer et al., 2015). Extreme precipitation occurs on different time and space scales: (a) long-lasting stratiform precipitation or (b) short-duration convective precipitation (e.g. Eggert et al., 2015). Type-(a) extremes typically cover extensive regions while type-(b) extremes occur more locally and randomly distributed.

To characterize a certain location with respect to its precipitation extremes it is necessary to determine the extremes for a range of aggregation times, e.g. from minutes to multi-days or even months. This requires temporally high-resolution rain measurements over long time periods but this is not often fulfilled. The most frequent time resolution of long time series is 1 day (e.g. Kunkel et al., 1999; Groisman et al., 2005; Zolina et al., 2009; van den Besselaar et al., 2012; Tammets and Jaagus, 2013). Increasingly, time series with sub-daily resolution in the range of hours to minutes are available (e.g. Kanae et al., 2004; Sen Roy and

*Corresponding author: Gerd Müller, Meteorological Institute, CEN, University of Hamburg, Bundesstrasse 55, 20146 Hamburg, Germany, e-mail: gerd.mueller@uni-hamburg.de

Rouault, 2013; Perez-Zanon et al., 2016, Blenkinsop et al., 2016) and recently also from rain-radar networks (e.g. Berg et al., 2013; Eggert et al., 2015). Beyond that, it is important to know how the extremes vary with aggregation time and how the individual aggregation-time extremes are distributed over the year and with daytime because this gives hints to the physical processes causing them.

The configuration of the large-scale atmospheric circulation plays a primary role for the formation of precipitation and extreme precipitation because it determines the presence or absence of the most important preconditions favouring precipitation such as increased moisture supply, reduced stability of vertical density stratification, and dynamically induced vertical lifting which can be caused by low-level convergence, by frontal processes, by warm-air advection, and by advection of vorticity in the upper troposphere. Of special importance is a conditionally unstable stratification because it is the crucial precondition for convective precipitation, whereas stratiform precipitation is generated when vertical lifting acts on air showing no conditional instability. In addition to the large-scale flow local characteristics such as orography, land-sea contrast or land use are important factors for the degree of extreme precipitation. A further parameter influencing extreme precipitation is the temperature or dew-point temperature level. The scaling of extreme precipitation with the Clausius-Clapeyron relation is discussed in the literature especially in the light of trends of extreme precipitation in a warmer climate (e.g. Berg et al., 2013; Westra et al., 2014). However, this aspect is not considered in this paper.

Considering the relation between large-scale circulation patterns and local precipitation is one method used for downscaling hydrological impacts of future climate scenarios, where downscaling stands for approaches to take information known at the large scale to produce predictions at local scales. There are essentially two downscaling methods. Dynamical downscaling requires running of a nested high-resolving model for a selected region of interest, but is computationally expensive. Statistical downscaling establishes links between local variables, as precipitation or temperature, and predictors representing large-scale weather. Predictors describing large-scale circulation patterns as well as other kinds of predictors revealing significant statistical relation between predictor and predictand can be used. Overviews on aspects of downscaling approaches are given by Fowler et al. (2007) and Maraun et al. (2010). Representation of sub-daily precipitation, especially extremes, from downscaling is still relatively poor and improvable (Maraun et al., 2010). Hence, increasing attention is put on downscaling with particular focus on extreme precipitation (e.g. Friedrichs, 2010; Müller et al., 2009; Gao et al., 2013; O'Gorman, 2015).

For the term "extreme" there is no fixed definition in the literature. The IPCC (2007) quite generally defines an extreme event as a rare event which occurs in only 10 % or even 1 % of the time. It is also pointed out that the absolute level above which precipitation is extreme depends on the region and the reference period. Peralta-Hernandez et al. (2009) give a good overview for different definitions of precipitation extremes and argue that conclusions on precipitation trends can be contradictory depending on which definition is used.

In this paper we present a precipitation statistics for one location, only. We use an up to 17-year long time series of precipitation amount and precipitation duration with 1 minute time resolution recorded at Hamburg, Germany. The paper has two objectives. The first objective is to derive for this location a set of comprehensive statistics for precipitation extremes. For this, we use the most frequent definition of extremes, namely the uppermost percentiles. We apply them to different aggregation times from minute to month and, thus, contribute new information on the sub-daily precipitation which is rarely measured (e.g. Kanae et al., 2004; Sen Roy and Rouault, 2013; Perez-Zanon et al., 2016) and is identified as a gap in precipitation measurements and thus in our knowledge on short-term precipitation statistics (e.g. Maraun et al., 2010; Westra et al., 2014). We distinguish the precipitation extremes for different seasons and times of the day. Thus, we are able to differentiate between the two main precipitation types, convective and stratiform, in the course of the year. We further study how the extremes vary with aggregation time and if they follow a scaling law such as the well-known Jennings law (Jennings, 1950).

The second objective of this paper is to find out which large-scale flow patterns favour extreme precipitation events. For this, we relate the precipitation extremes to the 40 weather types of the DWD (Deutscher Wetterdienst) objective weather type classification in order to test its potential to serve as downscaling predictor for extreme precipitation. We shall see that, although certain weather types dominate, the wide variety of weather types is surprising. We explore if, despite this variety, there are other overarching synoptic features favouring extreme precipitation but not represented by the objective classification.

The paper is organized as follows. In Section 2, the observation site, instrumentation, and our definition of extreme precipitation are presented. Furthermore, we describe the datasets used for the large-scale weather situation. In Section 3 the precipitation climatology is presented. This includes (a) inter-annual variations and the mean annual and diurnal cycles in order to place the results for the precipitation extremes in a wider context, (b) the frequency distributions and extremes of precipitation amount for different aggregation times, and (c) the analysis of the annual and diurnal variation of precipitation extremes. In Section 4, we investigate which weather types of the DWD classification are most favourable for the generation of convective and stratiform extreme precipitation in summer and winter and test the potential of the classification to serve as downscaling predictor for extreme precipitation.

2 Data and definitions

2.1 Location and instrumentation of Hamburg weather mast

Our investigations are based on measurements at the Hamburg Weather Mast which is located at 53.5192° N, 10.1029° E, about 8 km south-east of the Hamburg city centre. The surrounding is predominantly suburban and industrial west of the mast and predominantly rural east of it. The Hamburg Weather Mast is operated by the Meteorological Institute of the University of Hamburg. Since 1995 various meteorological parameters at 8 levels up to 280 m height have been recorded digitally in an enhanced temporal resolution up to one minute. The Weather Mast facility and a general climatologic overview for that site are presented in Brümmer et al. (2012).

In the following, we briefly describe the instrumentation which is used to measure precipitation amount and duration. Precipitation amount is sampled since July 1997 with a tipping bucket of manufacturer Lambrecht GmbH embedded in a heatable Hellmann rain gauge with a circle area of 200 cm^2 complient to WMO standards. The tipping bucket has a water capacity of 2 g corresponding to 0.1 mm precipitation. After being filled by water, the bucket tilts over and an electronic pulse is registered. Rain rates between 0.1 and 8.0 mm/min can be resolved. During heavy precipitation events an overrun of the tipping bucket can occur. This error was corrected in the dataset for precipitation intensities above 1.3 mm/min according to the manufacturer's calibration. The correction had to be applied for 106 individual minutes. Here, we use precipitation amount data with 1-min time resolution from July 1997 to June 2014 with an availability of 95.8 %.

Precipitation duration is measured with an infrared detector of the manufacturer Eigenbrodt (RLS IRSS-88) with a horizontal detection area of 12 cm × 3 cm. The instrument user has the free choice to set the minimum number of detected particles per minute to define this minute as a precipitation minute. Our setting is 5 detections per minute. Potential erroneous measurements (may be dust or blowing snow) have been excluded from evaluation in consequence of a quality check. Measurements of precipitation duration started not before July 2006. Here, we use precipitation duration data from July 2006 to June 2014 with an availability of 98 %.

All data, not only the precipitation data, from the Hamburg Weather Mast are transmitted online to the Meteorological Institute of the University of Hamburg and are daily checked and cross-checked against other measurements (e.g. ceilometer backscatter data and data from upward looking short- and long-wave radiometers) for plausibility to detect errors and to repair possible instrument failures soon. This is an important control step for a high data quality. All Hamburg Weather Mast data are displayed online under http://wettermast.uni-hamburg.de.

2.2 Definition of extremes and handling of missing data

We calculate precipitation extremes for different aggregation times (AT): AT = 1 minute, 10 minutes, 1 hour, 1 day, 5 days and 1 month. We use non-overlapping time intervals for all AT and, in addition, overlapping time intervals for AT=1 month and 5 days shifted by 1 day, for AT = 1 day shifted by 1 hour, and AT = 1 hour and 10 minutes shifted by 1 minute. All AT with precipitation sum (PS) equal to zero (PS = 0) are not regarded further. For the remaining ATs with PS > 0 we calculate frequency distributions and from these the 95th and 99th percentile values and the absolute maximum. These three values are referred to as "extremes" in this paper. In some papers (e.g. Groisman et al., 2005), the 95th percentile is called "heavy" precipitation and the 99th percentile "very heavy" precipitation.

We calculate the three extreme values for each AT for the entire measuring period (7/1997–6/2014) (we call them the "overall" extreme values). The three extreme values are also calculated for data subsets, e.g. the same months (e.g. all Januaries) or the same time of day (e.g. all hours from 10 to 11 CET), so that we are able to determine the annual and diurnal cycle of the three extremes, respectively. Additionally, we use the overall extreme values and count the number of cases exceeding them to determine the annual and diurnal cycle of extreme events.

The above-mentioned missing 4.2 % of 1-minute precipitation-amount data are distributed irregularly and with different durations over the 17-year time series. The main reasons for gaps are routine maintenance, repairing or power outage. Longer repair work took place in April 1998 and from February to April 2001. Two power outages of 2–3 weeks affecting the entire Hamburg Weather Mast facility occurred in August 1999 and July 2001 due to thunderstorm lightning. Breaking the 4.2 % missing data down to months the gaps vary between a minimum of 0.1 % in November and a maximum of 11.6 % in April.

For each AT a different method is used to handle missing 1 min-values in the precipitation time series. First, we mention that no missing 1-min value is replaced in the 1-minute time series. A valid AT = 10 min sum must consist of 10 correctly measured minutes. The same holds for a valid AT = 1-hour sum with 60 correctly measured minutes. We define an AT = 1-day sum as valid if the number of missing minutes does not exceed 120. Five-day sums consist of five consecutive valid day sums. To avoid a systematic underestimation of the monthly and annual precipitation totals due to missing day sums, gaps in the time series were filled with the mean 1-day value over all valid measurements for the respective month. The mean diurnal cycles and all calculated thresholds like percentile values are based on a population of all valid measurements for each AT. The distinctly smaller number (2 %) of missing rain-

Table 1: The objective DWD weather type classification is based on four indices. Upper part: The four indices and their classes. Combination of these indices results in $5 \times 2 \times 2 \times 2 = 40$ weather types. Lower part: The 40 weather types: numbering and corresponding five-character abbreviation. For example, weather type 25 = NWZAT indicates "northwesterly" flow at 700 hPa, "cyclonic" at 950 hPa, "anticylonic" at 500 hPa, and "dry".

Wind direction at 700 hPa (Character 1–2)	**Cyclonality at 950 hPa** (Character 3)	**Cyclonality at 500 hPa** (Character 4)	**Integrated precipitable water** (Character 5)
XX not defined NO Northeast SO Southeast SW Southwest NW Northwest	A anticyclonic Z cyclonic	A anticyclonic Z cyclonic	T dry F wet
01 XXAAT	11 XXAZT	21 XXZAT	31 XXZZT
02 NOAAT	12 NOAZT	22 NOZAT	32 NOZZT
03 SOAAT	13 SOAZT	23 SOZAT	33 SOZZT
04 SWAAT	14 SWAZT	24 SWZAT	34 SWZZT
05 NWAAT	15 NWAZT	25 NWZAT	35 NWZZT
06 XXAAF	16 XXAZF	26 XXZAF	36 XXZZF
07 NOAAF	17 NOAZF	27 NOZAF	37 NOZZF
08 SOAAF	18 SOAZF	28 SOZAF	38 SOZZF
09 SWAAF	19 SWAZF	29 SWZAF	39 SWZZF
10 NWAAF	20 NWAZF	30 NWZAF	40 NWZZF

duration data was treated with the same method as for rain amount.

2.3 Large-scale datasets

To relate an extreme precipitation event to the synoptic situation three large-scale meteorological datasets are used.

The first dataset is the output of the objective weather type classification used by the Deutscher Wetterdienst (DWD) to classify once per day the large-scale weather type (Dittmann et al., 1995; Bissolli and Dittmann, 2001). For this method the daily 12-UT analysis of the operational numerical weather-analysis and -forecast system of the DWD is used. Model data from a rectangular area with the corner points 55° 15′ N, 2° E and 55° 15′ N, 18° 20' E and 45°30' N, 3°45' E and 45° 30′ N, 16° 25′ E enter into the classification. The centre of the area is at 50° 24′ N, 10° E, thus, not at Hamburg but about 300 km south of Hamburg. The classification contains 40 weather types which are built on four weather-type classifying indices (Table 1). The first one represents five possible wind directions at pressure level 700 hPa (XX: not defined, NO: northeast, SO: southeast, SW: southwest, NW: northwest). The second index characterizes two possible states of cyclonality (A: anticyclonic, Z: cyclonic) at pressure surface 950 hPa, a height level typically located within the boundary layer. The same scheme is used for the third index characterizing cyclonality at pressure surface 500 hPa representing the vertical mid of the troposphere. The fourth index stands for two possible states of humidity of the atmosphere (T: dry, F: wet) derived from integrated precipitable water. Combination of area weighted means of these indices results in $5 \times 2 \times 2 \times 2 = 40$ large-scale weather types. For example, the classification NWZAT indicates weather type "northwest", cyclonic at 950 hPa, anticyclonic at 500 hPa, and dry. In contrast to subjective methods the objective weather type classification is unambiguously defined and at any time numerically reproducible with the same result.

The second dataset is the 6-hourly NCEP (National Centers for Environmental Prediction) reanalysis II with a horizontal resolution of 2.5°×2.5°. NCEP data are used to compute composites (averages) of the mean sea level pressure (SLP), the 850-hPa and 500-hPa geopotential height and the 850-hPa temperature for central Europe over those days between July 1997 and June 2014 showing a daily precipitation sum exceeding the overall 95$^{\text{th}}$ percentile over the entire period (07/1997–06/2014) of 13.8 mm/d at Hamburg Weather Mast.

The third dataset is the 6-hourly operational analysis charts of the weather prediction model GFS (Global Forecasting System) of the NCEP.

3 Climatology of observed precipitation amount and duration

3.1 Inter-annual variations and mean annual and diurnal precipitation cycles

After applying the "climatologic" gap substitution (Section 2.2) and using only the complete years 1998–2013 the annual mean amount is 704 mm/a. Regarding for precipitation duration only the complete years 2007–2013 the annual mean duration is 776 h/a or 8.8 % of time. The inter-annual variations of precipitation amount and duration are shown in Fig. 1. The standard deviation of annual precipitation amount is $\sigma_{PS} = +/-110$ mm/a and that of annual precipitation duration is $\sigma_{PD} = +/-80$ h/a. In the wettest year (2007) a precipitation amount of 940 mm was recorded. The maximum precipitation duration year was 2010 with 914 h or 10.4 % of time.

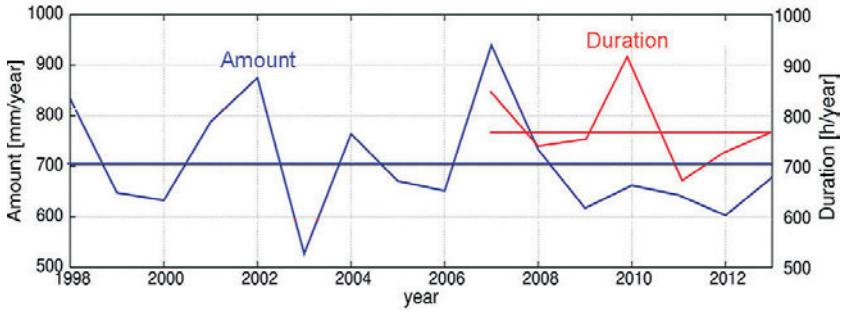

Figure 1: Annual precipitation amount and duration and corresponding mean values.

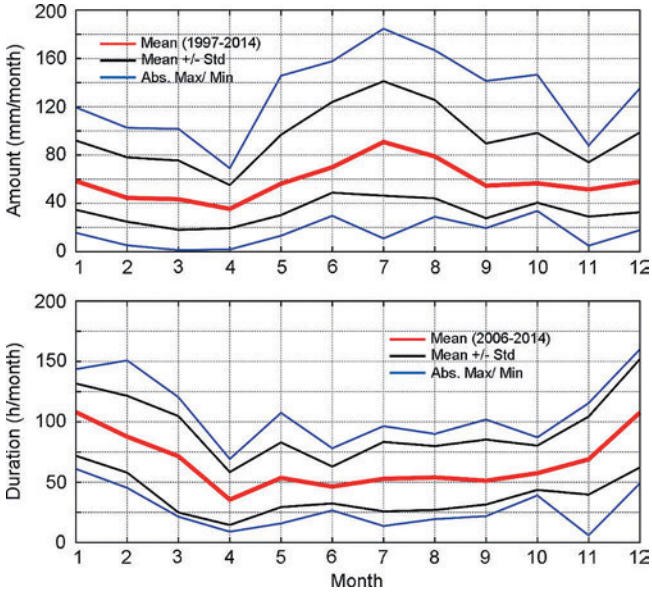

Figure 2: Annual cycle of monthly precipitation amount for 1997–2014 and monthly precipitation duration for 2006–2014.

The annual cycles of monthly mean precipitation amount and duration are shown in Fig. 2. On average, the monthly precipitation amount is largest in July (90 mm), smaller in winter and at a minimum in April (35 mm). The standard deviation has a similar annual course with the largest variability in summer. The mean annual course of precipitation duration is almost opposite to that of precipitation amount with most precipitation hours in winter (December/January ~ 109 h/month), less in summer (~ 50 h/month) and the minimum in April (~ 35 h/month). Thus, April is in both respects the driest month of the year. In contrast to precipitation amount, the standard deviation of precipitation duration is almost the same for all months.

The mean diurnal cycles of precipitation amount and duration in the four seasons are presented in Fig. 3. Only in summer, the precipitation amount shows a clear diurnal cycle with the largest values in the afternoon and early evening hours. Spring has a similar cycle but with a smaller amplitude, while autumn and winter show no variation of precipitation amount. Apart from the outstanding higher level of precipitation duration in winter compared to other seasons, precipitation duration shows no significant diurnal variation ($< +/-0.5$ min/h).

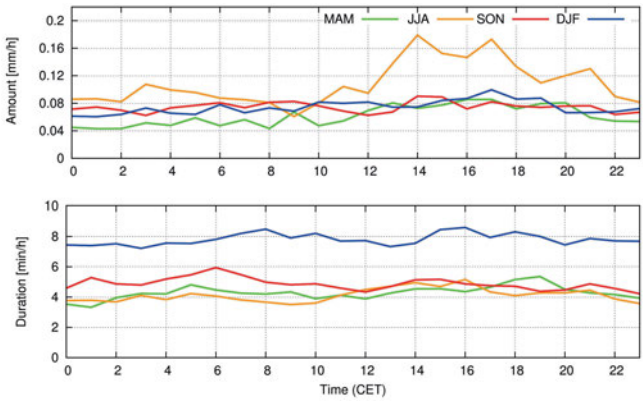

Figure 3: Mean diurnal cycle of hourly precipitation amount and precipitation duration in spring (MAM), summer (JJA), autumn (SON) and winter (DJF) based on all (wet and dry) times.

3.2 Precipitation PDF for different aggregation times

The overall (entire observation period) probability density functions (PDF) of precipitation amount for five different aggregation times (AT) are shown in Fig. 4. Monthly precipitation amount has a Weibull-like distribution (Gamma distribution on a 95 % significance level with a Chi^2 test) which peaks in the interval 40–50 mm/month. The three overall extremes, 95th, 99th and absolute maximum, are 135.8, 166.9, and 182.4 mm/month, respectively. The shape of the frequency distribution changes with decreasing AT. If AT = 5 days or shorter the density distribution peaks in the smallest class of precipitation sum. The contributions from the four seasons are almost the same for AT = 1 month and to some degree also for AT = 5 days and 1 day. But for shorter AT (1 hour to 1 minute), the contribution from the summer season becomes more dominant. Particularly the precipitation events on the high end of the distributions tend to be from summer events.

Important parameters characterising the precipitation statistics for each AT are summarized in Table 2. The portion of time with precipitation to the total time depends on the AT interval. It decreases from 100 % for AT = 1 month (there was no month without precipitation) to 5 % for AT = 10 min and even to 1.1 % for

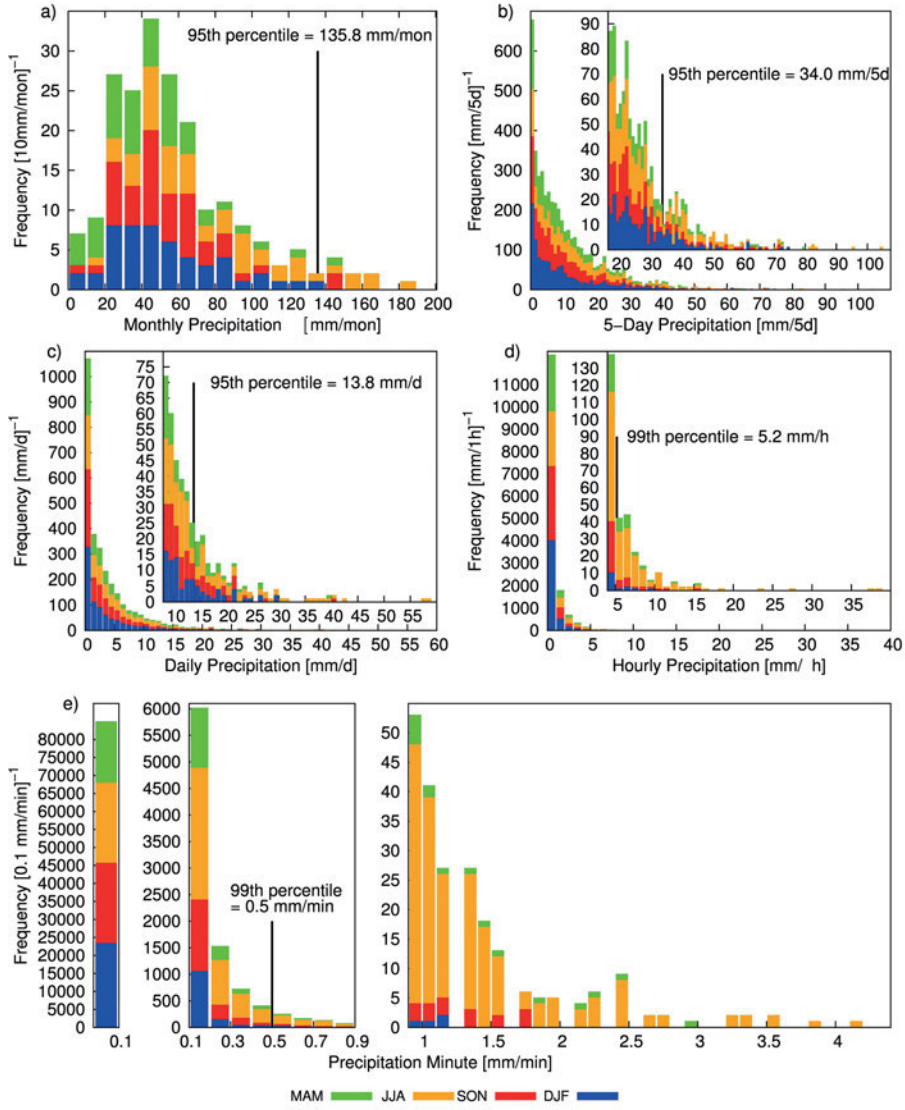

Figure 4: Frequency distribution of precipitation amount for AT = 1 month (a), 5 days (b), 1 day (c), 1 hour (d) and 1 minute (e) for the entire measuring period (7/1997–6/2014). Different colours indicate the contribution from each season. Black vertical line marks 95th or 99th percentile value.

Table 2: Summary of statistical quantities for different aggregation times (AT) from tipping bucket data (07/1997–06/2014). Values in brackets are from rain detector data (07/2006–06/2014). The absolute maxima are given for fixed non-overlapping AT and moving overlapping AT (moving steps are 1 day for AT = 1 month and 5 days, 1 hour for AT = 1 day, and 1 minute for AT = 1 hour and 10 minutes).

Aggregation Time		1 month	5 days	1 day	1 hour	10 min	1 min
Total Number		204	6209	6209	149016	894096	8940960
Missing Values		0	575	309	6898	37915	372422
Time portion with precip.	– Year (%)	100	85.5	49.4	10.9	5.0	1.1 (8.7)
	– MAM (%)	100	78.3	41.8	9.0	4.1	0.9 (7.1)
	– JJA (%)	100	87.9	49.6	9.8	4.6	1.3 (6.8)
	– SON (%)	100	86.8	51.5	11.2	5.4	1.1 (8.3)
	– DJF (%)	100	89.1	54.7	13.4	6.1	1.2 (12.9)
Mean (mm)		58.19	11.04	3.84	0.74	0.27	0.12
Median (mm)		50.0	7.5	2.0	0.3	0.1	0.1
Skewness		1.16	2.0	3.2	8.4	14.6	12.4
Curtosis		4.3	9	20	165	416	267
95thPercent. (mm)		135.8	34.0	13.8	2.6	0.8	0.2
99th Percent.(mm)		166.9	52.8	24.1	5.2	1.8	0.5
Abs. Max. (mm) (fixed interval)		182.4	92.4	58.2	38.2	19.9	4.2
Abs. Max. (mm) (moving interval)		259.0	104.6	73.4	51.6	23.6	4.2

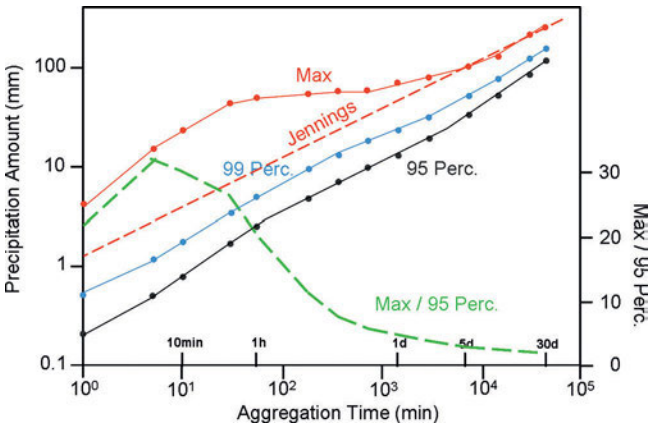

Figure 5: Precipitation amount versus aggregation time for the 95th and 99th percentile and the absolute maximum taken from the PDFs for the total 17-year period (left scale) and maximum/95th percentile ratio versus aggregation time (right scale). The red dashed curve shows the Jennings (1950) scaling power law with the exponent 0.50.

AT = 1 min based on the tipping bucket data. Due to the measurement method of the tipping bucket (it does not tilt over unless 2 g water are collected in the bucket) the precipitation portions based on AT = 1 and 10 min are underestimated. The rain detector delivers 8.7 % for AT = 1 min. This value is between the bucket values for AT = 1 h and 10 min. Thus, as a practical result, the tipping bucket can also be used for time portion estimates of precipitation if the AT is not shorter than about 30 min. Skewness and curtosis of the PDF increase with decreasing AT except for the shortest AT of 1 min. The absolute precipitation maxima for AT = 1 d and 1 h can be up to one third higher in case of overlapping instead of non-overlapping time intervals.

The 3 overall (total 17-year period) extremes are displayed as function of AT in Fig. 5 in a log-log plot. Interestingly, both the 95th and 99th percentile increase almost linearly, corresponding to power laws as

$$\text{Perc95(mm)} = 0.19\,\text{AT (min)}^{0.61} \qquad (3.1a)$$

$$\text{Perc99(mm)} = 0.48\,\text{AT (min)}^{0.55}, \qquad (3.1b)$$

valid for the range 1 min < AT < 30 d. Thus, as a practical result, if the 95th and 99th percentile values are known for only one AT (most long-term precipitation series are available for AT = 1d), they can be estimated for other AT from Equation (3.1). The overall maximum (moving overlapping intervals) is usually described by the Jennings (1950) power law with the exponent of 0.50 (e.g. Zhang et al., 2013). The Jennings law does not apply here; it underestimates the extreme values in the subdaily AT range, particularly below 1 h. This is probably a consequence of the different modes of precipitation: convective and stratiform. For the long AT range (AT > 5 d) both modes contribute to the maximum values while for the short AT range (AT < 1 h) convection exclusively causes the absolute maximum. The convection-mode maxima are "outsized" compared to the mixed-mode maxima. This is underlined in Fig. 5 by the ratio of the absolute maximum versus the 95th percentile value. The ratio is between 20 and 30 for AT < 1 h and between 3 and 1.5 for AT > 5 d. The ratio peaks for AT = 5–10 min (as do the skewness and curtosis values in Table 2). This indicates that the possible range of maximum precipitation within 1 minute is more limited than the possible range within 10 minutes. The maximum precipitation for AT = 1 min has only one degree of freedom, namely intensity, whereas for AT = 10 min it has two degrees of freedom, namely intensity and duration. Going to longer AT, it is unlikely that extreme precipitation intensity lasts for a full hour, thus, making the maximum/95th percentile ratio smaller again.

3.3 Annual cycle of precipitation extremes

The annual cycles (monthly subsets) of individual precipitation extremes (95th and 99th percentile and absolute maximum) for AT = 1 d, 1 h and 1 min are presented in Fig. 6 (left column). All three extreme values exhibit a maximum in the summer season for all three AT; July is the preferred month for the maximum. The winter extremes are clearly smaller by a factor of about 1/2 for AT = 1 d and even of about 1/4 for AT = 1 h and 1 min. This underlines the preferred occurrence of convective precipitation in the summer season and agrees with the findings of Blenkinsop et al. (2016) who analysed AT = 1-h data for the United Kingdom.

This annual course of precipitation extremes is even more distinctly emphasized when considering the numbers of cases exceeding the overall extreme values for AT = 1 d (13.8 mm/d), AT = 1 h (5.2 mm/h) and AT = 1 min (0.5 mm/min) as shown in the right column of Fig. 6. While for AT = 1 d the maximum-to-minimum ratio of exceeding cases is about 5:1, it is about 50:1 for AT = 1 min. Thus, we conclude that short-term extremes (AT = 1 min) are likely solely of convective origin whereas medium-term extremes (AT = 1 d) can result from both short convective events and longer-lasting frontal (stratiform) events. This conclusion is supported when comparing the individual monthly absolute maxima for AT = 1 h with the overall 95th daily percentile of 13.8 mm/d. The 1-h absolute maximum exceeds the overall 1-d extreme in all months from May to September but stays below it from October to April.

3.4 Diurnal cycle of precipitation extremes

The diurnal cycles (hourly subsets) of individual precipitation extremes (95th and 99th percentile and absolute maximum) for AT = 1 h and 1 min are shown in Fig. 7. To contrast the seasonal differences of precipitation, we present the diurnal cycles for the summer and winter season, only.

In the winter season we find no significant diurnal cycle of extreme precipitation. Neither the 95th and

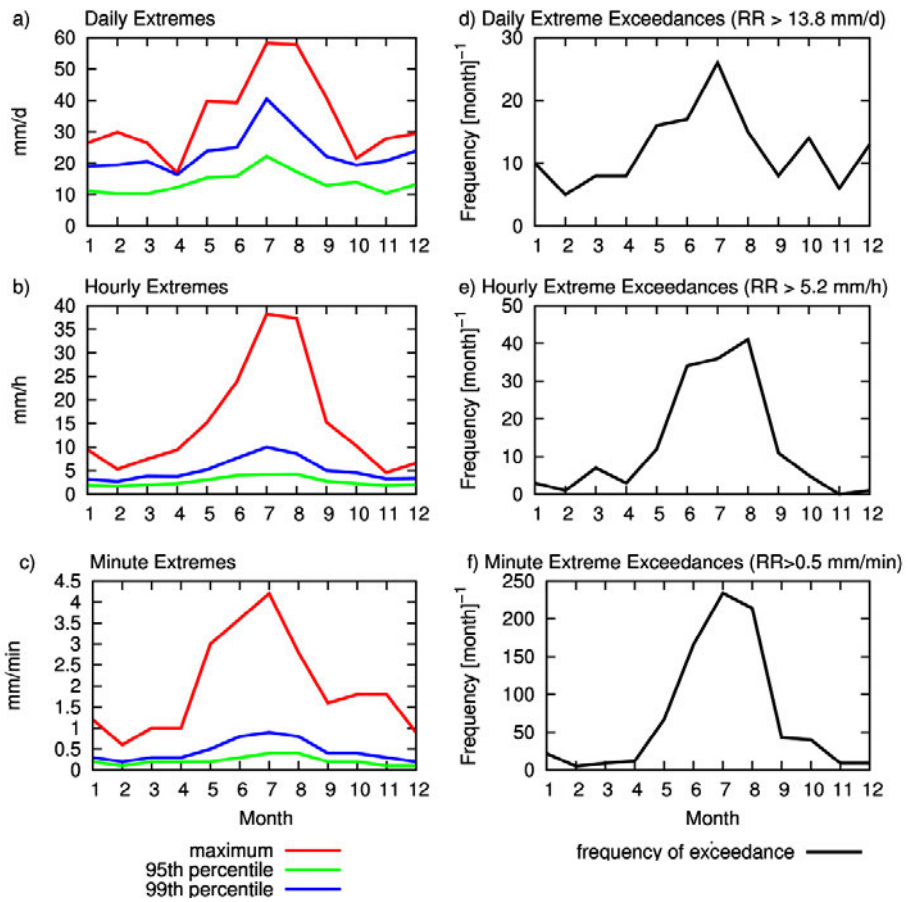

Figure 6: Left column: Annual cycle (monthly intervals) of individual 95th and 99th percentile and maximum of precipitation sum per (a) day, (b) hour and (c) minute. Right column: Annual cycle (monthly intervals) of exceeding numbers of the (d) overall 95th percentile of precipitation per day (13.8 mm/d), (e) overall 99th percentile of precipitation per hour (5.2 mm/h) and (f) overall 99th percentile of precipitation per minute (0.5 mm/min).

99th percentiles nor the exceeding frequencies for both AT = 1 h and AT = 1 min show any remarkable variation in the course of the day. In the winter season the influence of solar radiation on convection is too small: daytime is only 7–8 h long and the measured mean noon maximum of down-welling short-wave radiation is only 140 W/m^2 (Brümmer et al., 2012).

The situation is different in summer. There is a clear diurnal cycle. It is particularly distinct for the 99th percentile, the absolute maximum and also for the exceeding frequencies for both AT = 1 h and AT = 1 min. The largest 99th percentile is three times (two times) higher than the overall 99th percentile for AT = 1 h (AT = 1 min). The maxima of extreme precipitation and exceeding frequency occur between 14 and 18 CET (Central European Time), but high values also extend into the night hours. This is a clear signal of the influence of solar radiation acting towards a destabilization of the vertical density stratification. Daytime hours amount to about 15 h (two times longer than in winter) and the measured mean noon maximum of down-welling short-wave radiation is 550 W/m^2 (four times more than in winter) (Brümmer et al., 2012).

4 Extreme precipitation and relation to large-scale weather situation

4.1 DWD weather types during extreme precipitation

(a) General frequency of DWD weather types

The general occurrence frequency of each DWD weather type is presented in Fig. 8 (for weather type notations see Table 1). The Figure refers to the same time period from July 1997 to June 2014 as covered by the precipitation measurements at the Hamburg Weather Mast. It is not surprising that the most frequent weather types are westerly patterns. The total relative frequencies of flow patterns are: southwest 37 %, northwest 29 %, northeast 8 %, southeast 6 %, not-defined 20 %. Concerning cyclonality, the percentages are distributed as follows: AA 41 %, AZ 25 %, ZA 16 % and ZZ 18 %. Thus, anticyclonic conditions at low and upper levels predominate, whereas pure cyclonic conditions are much less frequent. Dry (T) and wet (F) conditions almost balance: T 52 % and F 48 %.

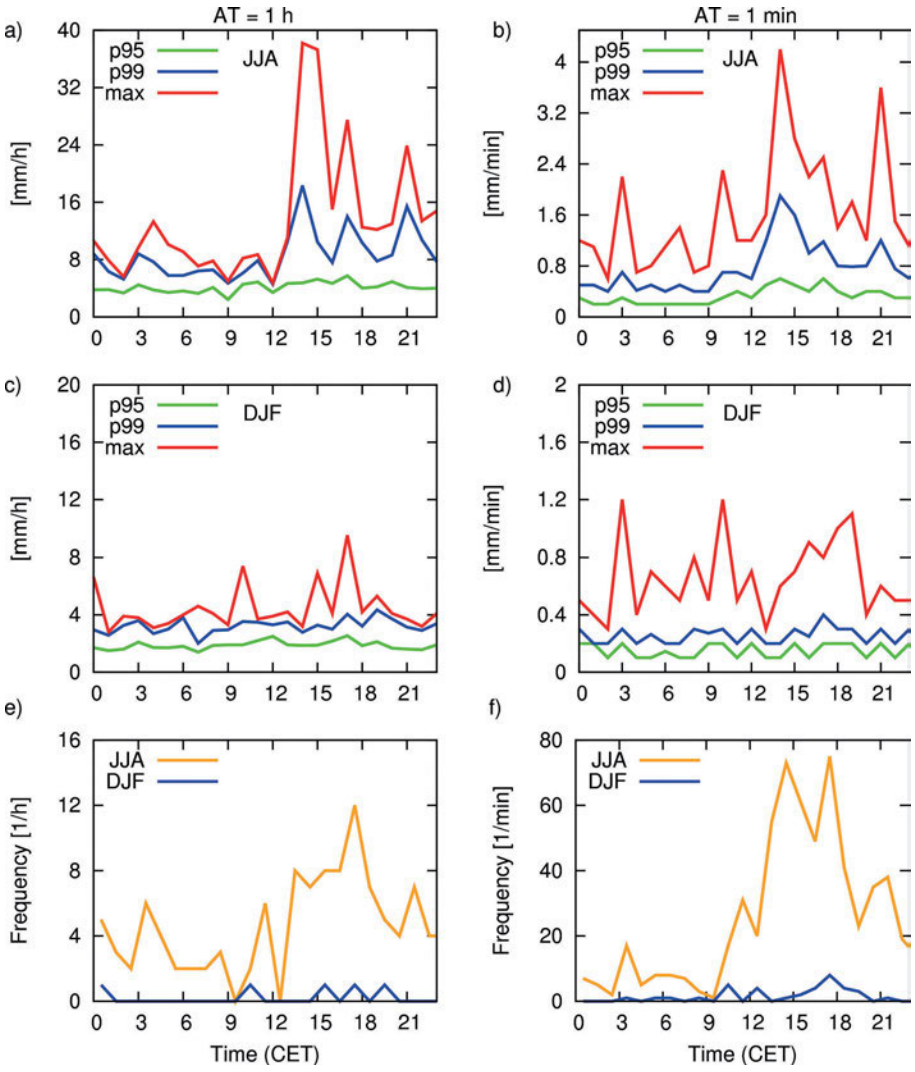

Figure 7: Left column: Diurnal cycle (hourly intervals) of the 95th and 99th percentile and the absolute maximum of precipitation amount per hour for summer JJA (a) and winter DJF (c); diurnal cycle (hourly intervals) of exceeding frequency of overall 99th percentile of 5.2 mm/h for summer and winter (e). Right column: (b, d) as left column (a, c) but for precipitation amount per minute; (f) as left column (e) but for overall 99th percentile of 0.5 mm/min.

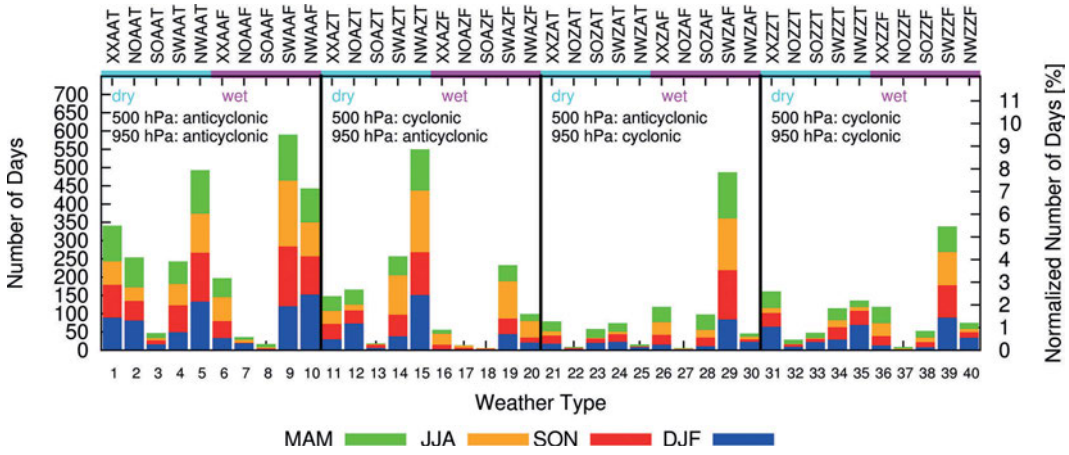

Figure 8: Absolute frequency distribution of the 40 large-scale weather types determined objectively by DWD for each day (valid for 12 UT) during the time interval July 1997 to June 2014 (6205 days.) Colours refer to seasonal contributions.

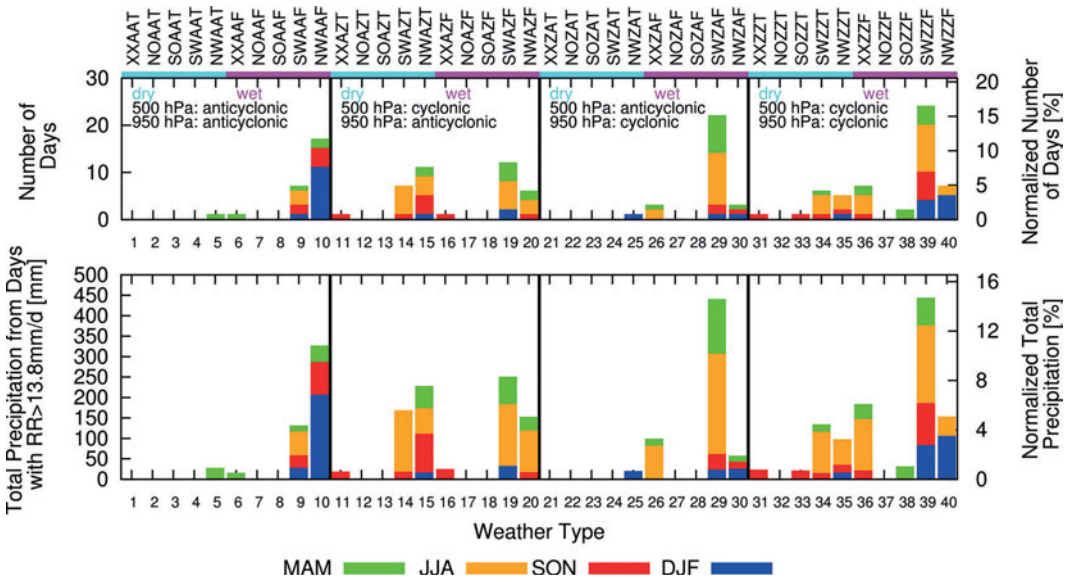

Figure 9: Number of extreme precipitation days (above) exceeding the overall 95th percentile of 13.8 mm/d and corresponding accumulated precipitation (below) in relation to the 40 large-scale weather types for the time interval July 1997 to June 2014. The scale on the right side is normalized with the total number of 146 days with > 13.8 mm/d and the total precipitation of 3021 mm during these days. Colours refer to seasonal contributions.

(b) Weather types during extreme daily precipitation

Fig. 9 (upper panel) shows for each weather type the frequency of days when precipitation exceeds the overall 95th percentile of 13.8 mm/d. Extreme precipitation days show up in 22 of 40 weather types. All north-easterly and south-easterly weather types are associated with no or few extreme precipitation days. Regarding the preferred weather types (occurring at least 4 times with extreme events) in each season, we find in spring south-westerly weather types 29 (8; 6.4 %), 19 (4; 9.1 %), 39 (4; 5.7 %), in summer south-westerly 29 (11; 7.7 %), 39 (10; 11.0 %), 19 (6; 5.9 %), 14 (6; 5.6 %), and not defined 36 (4; 11.4 %), in autumn south-westerly 39 (6; 6.7 %), and north-westerly 15 (4; 3.4 %), 10 (4; 3.8 %), and in winter the north-westerly 10 (11; 7.3 %), 40 (5; 15.6 %), and south-westerly 39 (4; 4.6 %) ranked with the number of extreme events as given by the first number in brackets. The second number in brackets gives the probability that an extreme event occurs when this weather type occurs. For all weather types the probability is rather small with a maximum of 16 %. The variety of preferred weather types is largest in summer.

Concerning the precipitation accumulated by the extreme events (Fig. 9; lower panel), the most outstanding result arises from weather type 10 (NWAAF) delivering extreme daily precipitation predominantly in winter and to a lower extent in the adjacent seasons but nothing in summer. The counterpart is weather type 29 (SWZAF) delivering more summer-time and spring-time extreme daily precipitation than all other weather types but almost nothing in winter. Also important is type 39 (SWZZF) although seasonal dependency is less pronounced.

To get more insight into these three outstanding weather types the underlying synoptic situations are presented in Fig. 10 as composite (average) fields of sea-level pressure and 500 hPa geopotential height derived from the 6-hourly NCEP re-analyses. For each day all four 6-hourly NCEP re-analyses entered into the composite. In order to see if days with and without extreme precipitation differ separate composites are calculated as well as the difference (days with minus without extreme precipitation).

The winter weather-type 10 (NWAAF) extreme precipitation composite (middle row, left in Fig. 10) is characterized by a straight zonal flow pattern with strong gradients at the surface and 500 hPa above Hamburg. The north-westerly component at higher levels (not very pronounced) is caused by a long-wave ridge with its axis extending from Iberia to Denmark giving the jet a slight anticyclonic curvature. Hence, the upper air flow delivers no dynamically driven mechanism for vertical lifting. But advection of warm air, the second driving mechanism for large-scale vertical lifting might be active. In this case it is very likely that extreme daily precipitation at Hamburg is due to long-lasting moderate precipitation below a flow-parallel and stationary (with respect to front-normal advancement) frontal zone separating cold air in the north from warmer air in the south. When comparing this with the type 10 winter-time composite from days without extreme precipitation (upper row, left) or viewing the plot of differences (lower row, left), respectively, it shows up that extreme precipitation is related with increased pressure gradient near surface and at upper level resulting in a stronger jet and near-surface flow, i.e. with an extraordinary sharply marked frontal zone located over Hamburg. The origin of the large-scale flow towards Hamburg is shifted towards south-west. This makes sense because a more southerly origin of the air

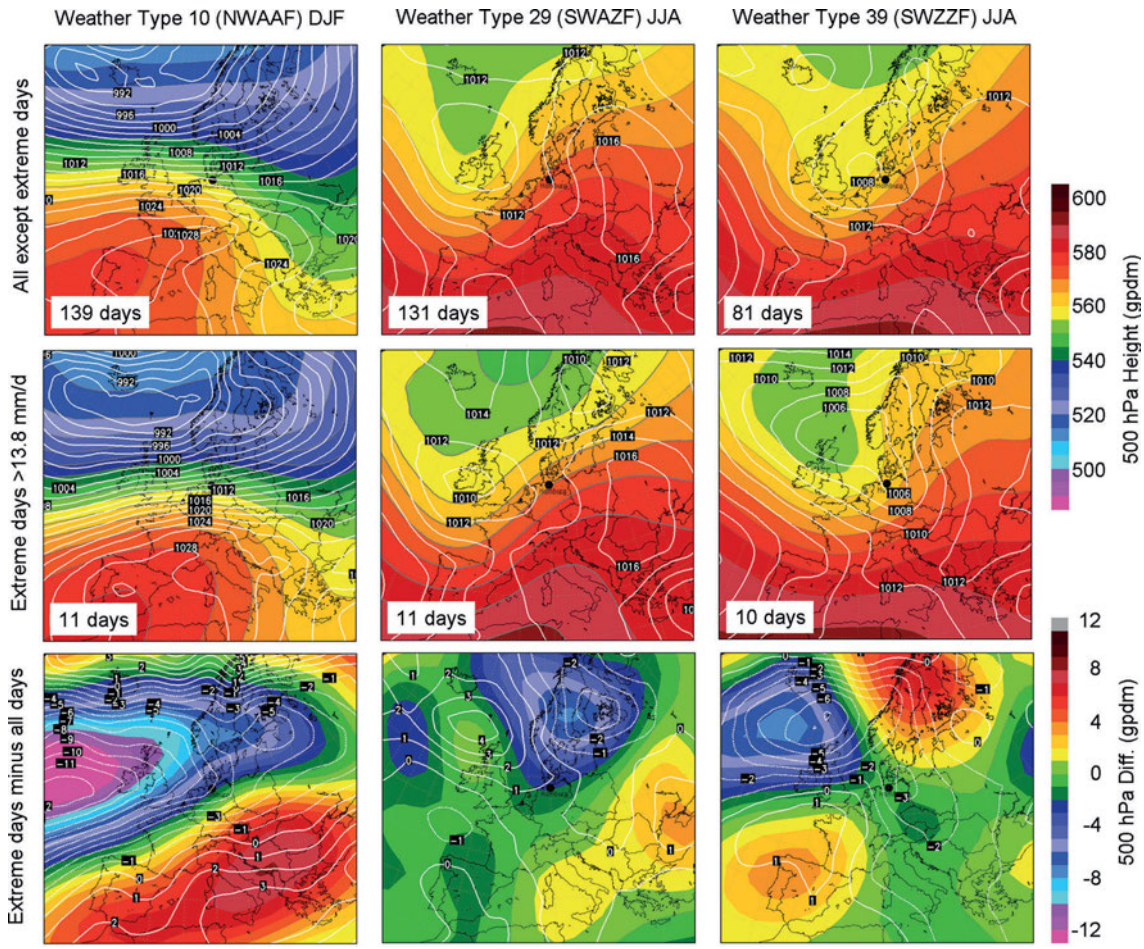

Figure 10: Composites of NCEP sea-level pressure (white isobars) and 500 hPa geopotential height (coloured) for the three most frequent weather types occurring with extreme daily precipitation (> 13.8 mm/d): weather type 10 (NWAAF) in winter (left column), weather type 29 (SWZAF) in summer (middle column) and weather type 39 (SWZZF) in summer (right column). Composites represent all days excluding the extreme days (upper row), only the extreme days (middle row) and the difference of extreme days minus all days (lower row). Numbers of days flowing into the composites are indicated. Black dot marks Hamburg.

mass from areas west of the Iberian Peninsula indicates more load of water vapour. These crucial aspects are not captured by objective weather type classification which only looks on flow curvature and direction over central Germany. The index F = wet is a helpful indication, but classification allowing only discrimination of wet and dry seems to be too coarse.

For the summer weather-type 29 (SWZAF) extreme-precipitation composite (Fig. 10, middle row, mid) the situation is different. This is a classical synoptic situation showing high potential for severe thunderstorms over Germany (e.g. Kurz, 1998). Hamburg is located ahead of the axis of a sharply marked upper-air trough in warm and moist air (large precipitable water load) of southerly origin typically showing more or less conditionally unstable stratification in summer. Vertical lifting prone to trigger convective events is generated ahead of the trough by advection of positive vorticity. The risk of severe-character convective developments is controlled by vertical wind shear. Strong upper-air flow (jet-stream over Germany) over weak near surface wind (weak surface gradient) would be an alarm signal for forecasters, the veering of direction from south-east (surface) to south-west (upper levels) increases the risk. The potential for organized convection as multi-cell thunderstorms, squall-lines and even super cells would be given in such a situation. The risk of a large precipitation amount is somewhat reduced due to relatively strong storm motion speed (similar to mean wind between 2 and 6 km height).

The composite of the second-frequent summer weather type 39 SWZZF (middle row, right) resembles the corresponding extreme-precipitation type 29 composite. In fact, the type 39 composite looks almost as type 29 composite at a later stage of development. The upper-air trough has moved eastwards and is closer to Hamburg. As a result upper-air flow curvature has changed from (slightly) anticyclonic to cyclonic, the only difference in classification indices. The surface trough is now fully developed and located near Hamburg. The configuration is a perfect trigger of convective showers and thunderstorms, all driving mechanisms discussed in the above paragraph are active, now even more exactly above Hamburg.

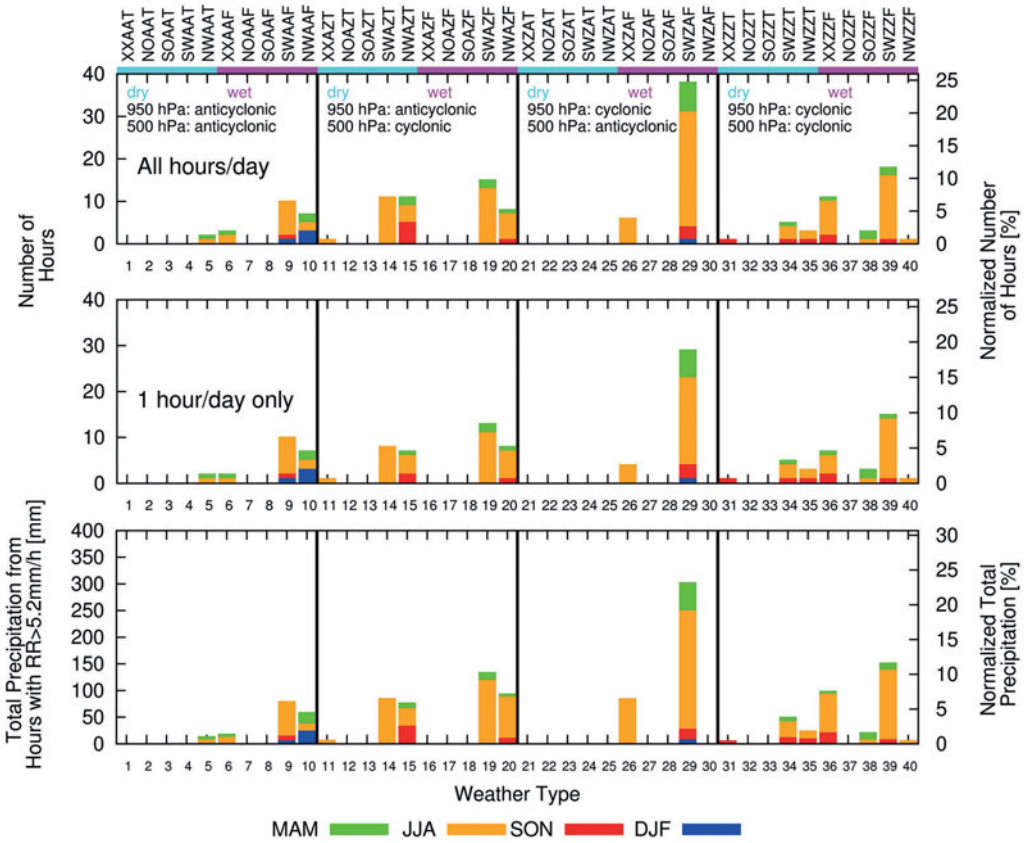

Figure 11: Number of extreme hourly precipitation events exceeding the overall 99th percentile of 5.2 mm/h with (above) and without (middle) multiple counting per day and corresponding accumulated (all hours) precipitation (below) in relation to the 40 large-scale weather types for the time interval July 1997 to June 2014. The scale on the right side is normalized with the total number of 154 hours with > 5.2 mm/h and the total precipitation of 1304 mm during these hours. Colours refer to seasonal contributions.

On the first glance there is surprisingly little difference when comparing the heavy-rainfall composites of type 29 and 39 with the corresponding ones of days without heavy rainfall. The main difference is in both cases a stronger jet velocity above Hamburg and increased low-level cyclonic curvature around Hamburg for heavy-rain days. Furthermore type 39 heavy-rainfall days are characterized by increased geopotential height over Scandinavia causing increased upper-air cyclonic curvature above northern Germany. This is plausible because these aspects are related with increased vertical lifting.

The classification of the weather-type 10 composite (left column in Fig. 10) as NWAAF is somewhat confusing because the composite of cases with and without extreme precipitation show in the large scale neither a clear northwest flow situation nor a clear anticyclonic curvature at 950 and 500 hPa. Instead, it is a straight zonal westerly situation. However, westerly flow is not a separate class in the DWD classification, but the crucial aspect which is an elongated west-east frontal zone with jet near Hamburg allowing long lasting precipitation is obviously well met when central Germany fulfils NWAAF conditions. The crucial aspect to catch cases with extreme precipitation, which are an extraordinary sharply marked frontal zone near Hamburg and increased load of precipitable water due to a more southerly origin of air mass, cannot be captured by the objective weather type classification indices. This could be overcome by taking into account large-scale pressure configuration, but also, more easily, by taking into account upper air wind velocity as indicator for the sharpness of the frontal zone and by including a more detailed humidity classification than a simple classification as wet and dry. On the other hand, the weather-types 29 and 39 composites clearly fulfil what is expected from a south-westerly flow situation and both types are nothing else than the same synoptic situation at different times of development. Also in these both cases the inclusion of upper air wind speed would do a good job in order to discriminate extreme from non-extreme precipitation days. In case of type 39 filtering out extreme-precipitation days could additionally be improved by taking into account the magnitude of upper-air cyclonality.

(c) Weather types during extreme hourly precipitation

Fig. 11 shows the frequency of weather types (with and without multiple counting per day) for only those days when hourly precipitation exceeds the overall 99th percentile of 5.2 mm/h.

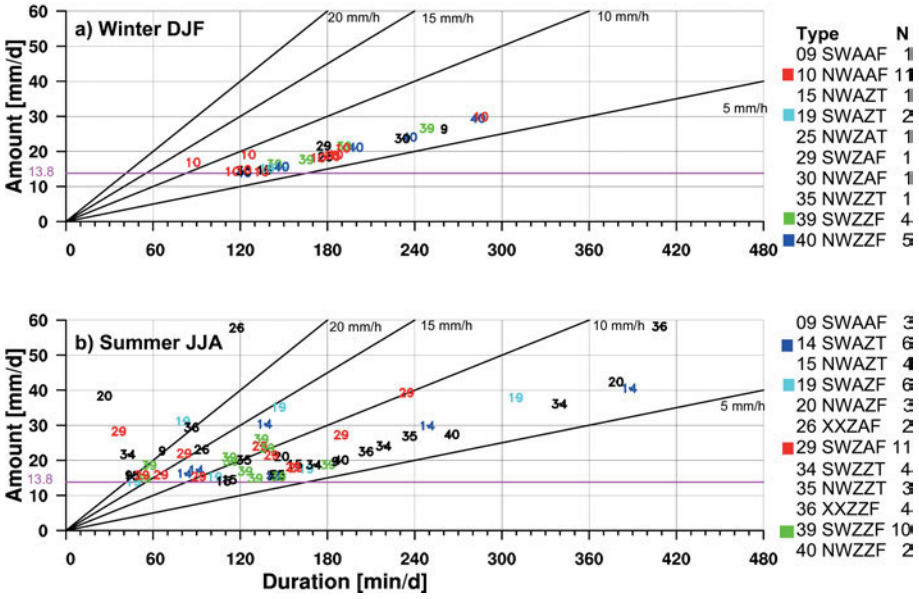

Figure 12: Precipitation amount vs. duration for all days exceeding the 95th percentile of 13.8 mm/d in winter (28 days; above) and summer (58 days; below). The numbers refer to the DWD weather type. The table on the right lists the weather types involved and their occurrence frequency N.

Also the corresponding total precipitation is displayed. Extreme hourly precipitation occurs predominantly in summer when precipitable water load and destabilizing impact of solar surface heating are larger than in other seasons. The most frequent weather types are the same as for extreme daily precipitation in summer (compare Fig. 9). The number of extreme hourly cases and the probability for extreme hourly precipitation when these weather types occur are as follows (only those weather types with more than 10 extreme cases are listed): weather type 29 (27 cases; 19 %), 39 (15; 16 %), 19 (13; 13 %) and 14 (11; 10 %). All weather types are south-westerly types with cyclonic flow either at 950 hPa (29) or 500 hPa (14, 19) or at both levels (39). The probability for an hourly extreme is clearly higher (order of factor 2) than for a daily extreme when one of these weather types occurs (cf. Section 4.1.b).

Concerning the outstanding north-western weather type 10 it can be confirmed that it is not much of a trigger of winter-time extreme hourly precipitation events (although there are three cases). Its large contribution to winter-time daily extreme precipitation as displayed in Fig. 9 is to a very large extent due to non-convective precipitation.

4.2 Distinguishing stratiform and convective extreme daily precipitation events

To distinguish daily extreme events (> 13.8 mm/d) of stratiform and convective origin we look at the relation between precipitation amount and duration which is presented separately for winter and summer in Fig. 12. For precipitation duration we use here the tipping bucket data since they are available for the entire 17-year observation period.

Interestingly, all 28 winter 1d extreme events are distributed in a relatively narrow sector of precipitation intensity around 7 mm/h. Thus, extreme precipitation intensity does not vary much and, therefore, the amount of extreme precipitation depends on the duration of the rain-producing synoptic situation. This hints at precipitation of primarily stratiform origin. The maximum daily amount in winter does not exceed 30 mm.

The amount-duration diagram for the 58 extreme summer events shows a more complex relation. On the one hand, there are, as in winter, many events which follow a linear amount-duration relationship with interestingly the same precipitation intensity. This hints again at stratiform precipitation. However, these stratiform summer events can last longer and thus reach daily precipitation amounts of almost 60 mm. On the other hand, there are many extreme daily summer events with short precipitation duration of less than 2 hours but with precipitation intensities > 15 mm/h. We assume that these are convection-dominated events. Independent of the season and precipitation mode (convective/stratiform), Fig. 12 generally shows that daily extreme events are related to a variety of DWD weather types.

4.3 Search for overarching features in extreme events producing weather types

As a result of the variety of DWD weather types involved in daily extreme events we investigate if any other overarching large-scale features can be found which are not covered by the four indices (wind direction, cyclonality at 950 and 500 hPa, and humidity) of the classification scheme. To this end, we inspect the 9 most extreme events (corresponding to recurrence times

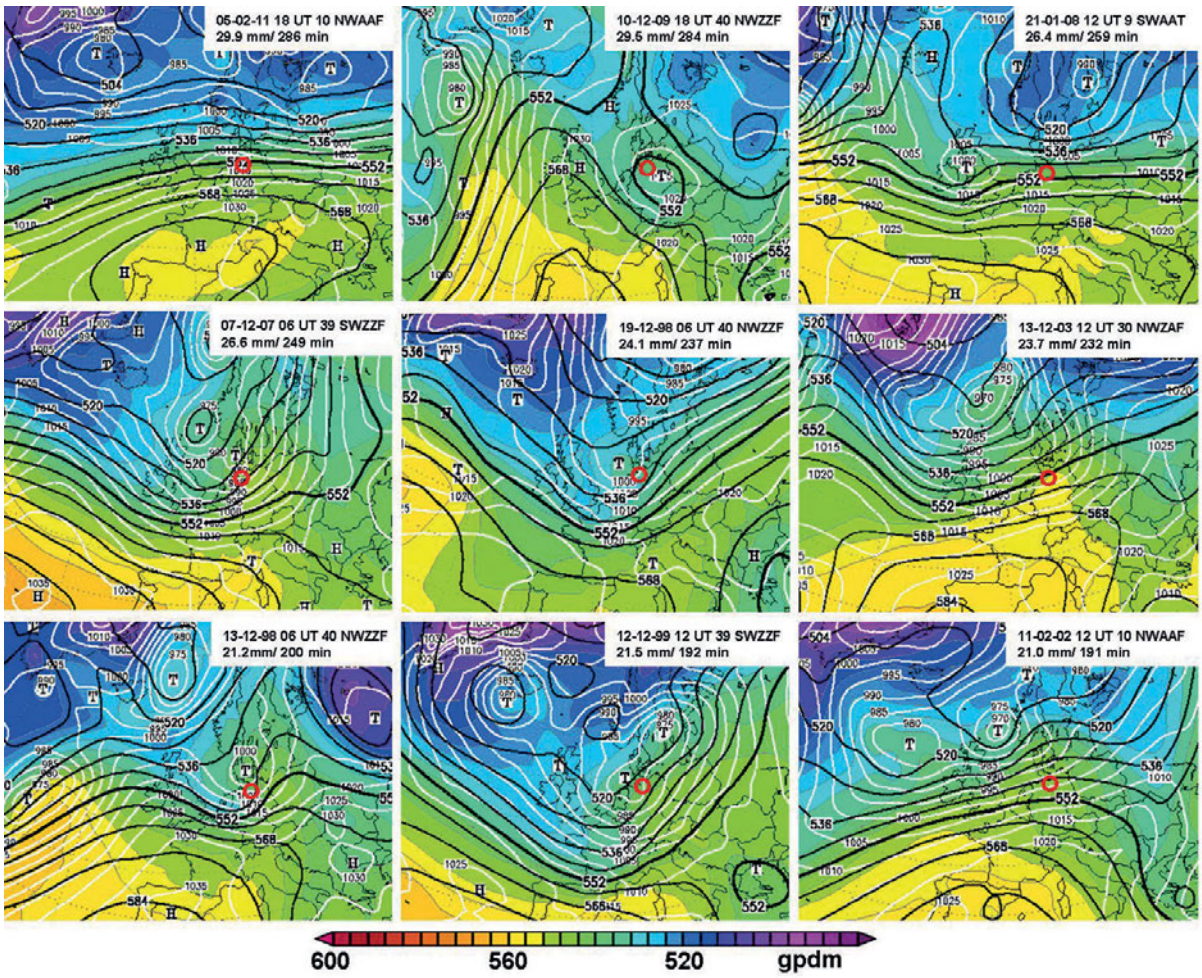

Figure 13: GFS analysis charts for the nine most extreme winter-stratiform precipitation events ranked in decreasing order according to the daily rain amount: sea-level pressure in white, 500-hPa geo-potential height in black, relative topography 500 hPa minus 1000 hPa in colours. The inset lists date, analysis time (UT), weather type, daily precipitation amount and duration.

of about two years or longer for our 17-year long observation period) of winter-stratiform, summer-stratiform and summer-convective precipitation separately and individually.

(a) Extreme winter-stratiform events

The nine most extreme winter-stratiform events are composed in Fig. 13. They have been selected from Fig. 12 under the condition of rain intensity between 5 and 8 mm/h and are ranked in decreasing order according to the daily rain amount. For each of the nine events that 6-hourly available GFS weather chart has been chosen which is closest in time to the beginning or already ongoing stratiform rain period. Note that these times can differ from 12 UT, the time for which the daily DWD weather type classification is valid.

Five different DWD weather types are involved in the nine strongest winter-stratiform cases. Nevertheless, they have several common synoptic features. In all nine cases the large-scale flow has a westerly component and transports moist air from the North Atlantic to the Hamburg region. With the exception of case 2, the jet stream marking the polar front between warm and cold air is above or south of Hamburg. The jet stream band has two different configurations. Either it has a long extension with almost no curvature which hints at little cross-jet band propagation or it is in the stage of developing a trough upstream of Hamburg which hints at vertical lifting above Hamburg.

Jet stream and trough are important features for wintertime stratiform precipitation extremes. The feature "jet stream" cannot be detected by the DWD classification because it does not contain any measure of upper-level wind speed. Also the feature "trough" is not clearly detected. This would require a measure for cyclonality. As mentioned above, taking into account upper-air wind speed and the magnitude of cyclonality would help to separate the strong cyclonic cases such as troughs.

(b) Extreme summer-stratiform events

The most extreme nine summer-stratiform events are presented in Fig. 14. They have also been selected from Fig. 12 under the condition of rain intensity between 5

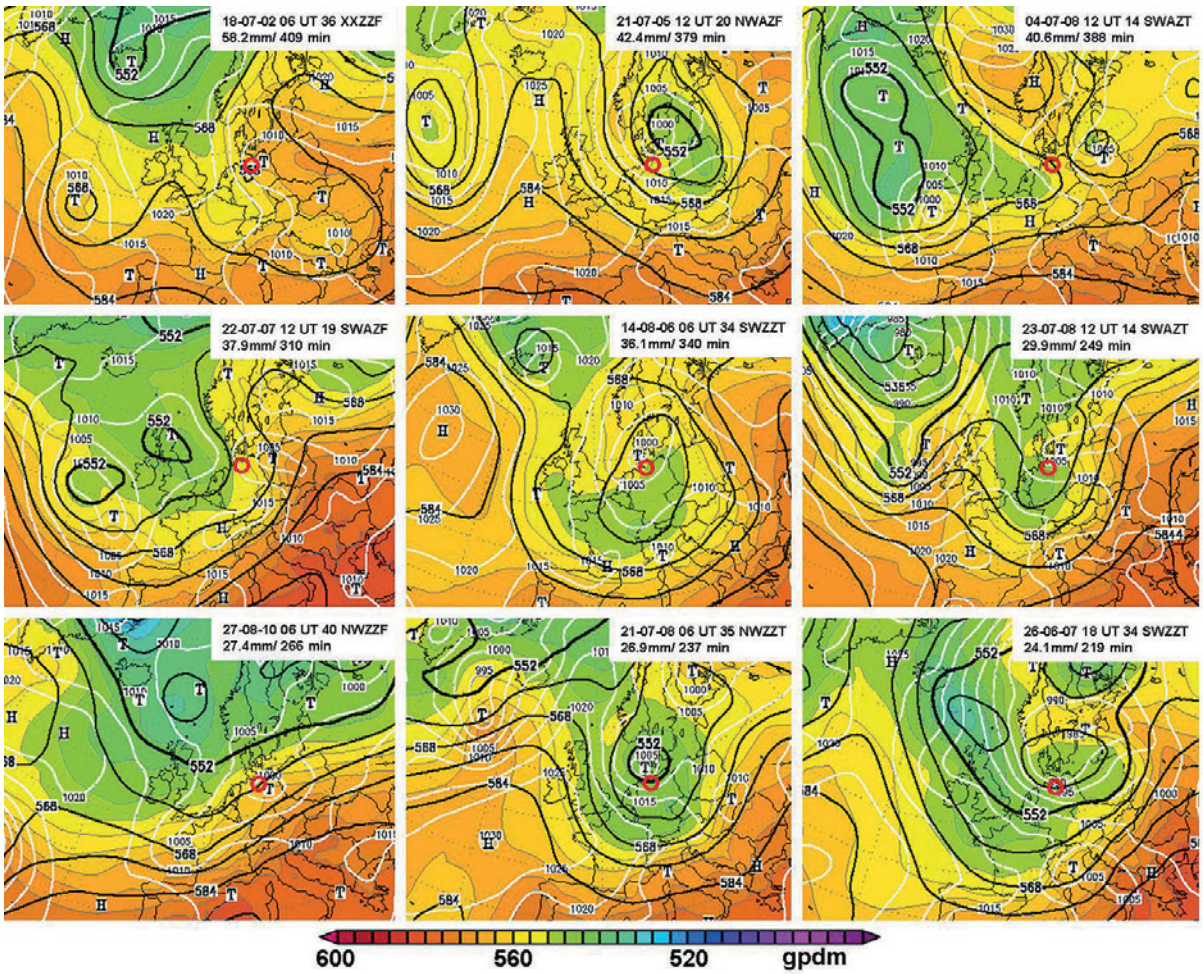

Figure 14: As Fig. 13, but for the nine most extreme summer-stratiform precipitation events.

and 8 mm/h and are ranked in decreasing order according to the daily rain amount. The nine strongest summer-stratiform cases occur with six different DWD weather types although the large-scale flows show similarities.

Except for case 7 which resembles a winter-stratiform situation, the upper-level circulation in all other cases shows a slowly propagating (information taken from the 6-hourly GFS charts) trough or cut-off low situated near Hamburg. On its eastside a surface low is generated which moves to a position east/northeast of Hamburg. This flow configuration leads to cold-air advection from the North Sea at low levels while warm air which was transported ahead of the upper-level trough far northward to Scandinavia glides on top of the low-level cold air and causes long-lasting stratiform precipitation. From Fig. 14 we conclude that three synoptic conditions are important for extreme summer-stratiform precipitation: "slowly-moving upper-level trough", "surface low at special position northeast of Hamburg", "differential temperature advection with height". These features are not captured by the DWD classification.

(c) Extreme summer-convective events

The nine most extreme summer-convective events are presented in Fig. 15. They have been selected from Fig. 12 under the condition of rain intensity higher than 15 mm/h and are ranked in decreasing order according to the daily rain amount. Although the nine cases are assigned to seven different DWD weather types, eight types indicate moist conditions with index F (wet). Furthermore, in all cases Hamburg is situated east of an upper-level trough/ low in a warm upper-level flow from southwest to southeast direction. The surface pressure gradient around Hamburg is small, but a weak surface low has formed near-by in some cases. In most cases the upper level jet is relatively strong and the relative topography 500 hPa minus 1000 hPa shows a strong temperature gradient zone west of Hamburg indicating an approaching cold front which brings a warm weather phase to an end.

The flow configurations during the extreme summer-convective events (Fig. 15) look not much different from those during the extreme summer-stratiform events (Fig. 14). The trough is further west for the convective events than for the stratiform events. Figs. 14 and 15 suggest as if the summer-convective events represent a flow situation occurring some time (12 to 24 hours) before the summer-stratiform situation. This idea is additionally supported by the fact that in some cases a weak surface low has already formed in the summer-

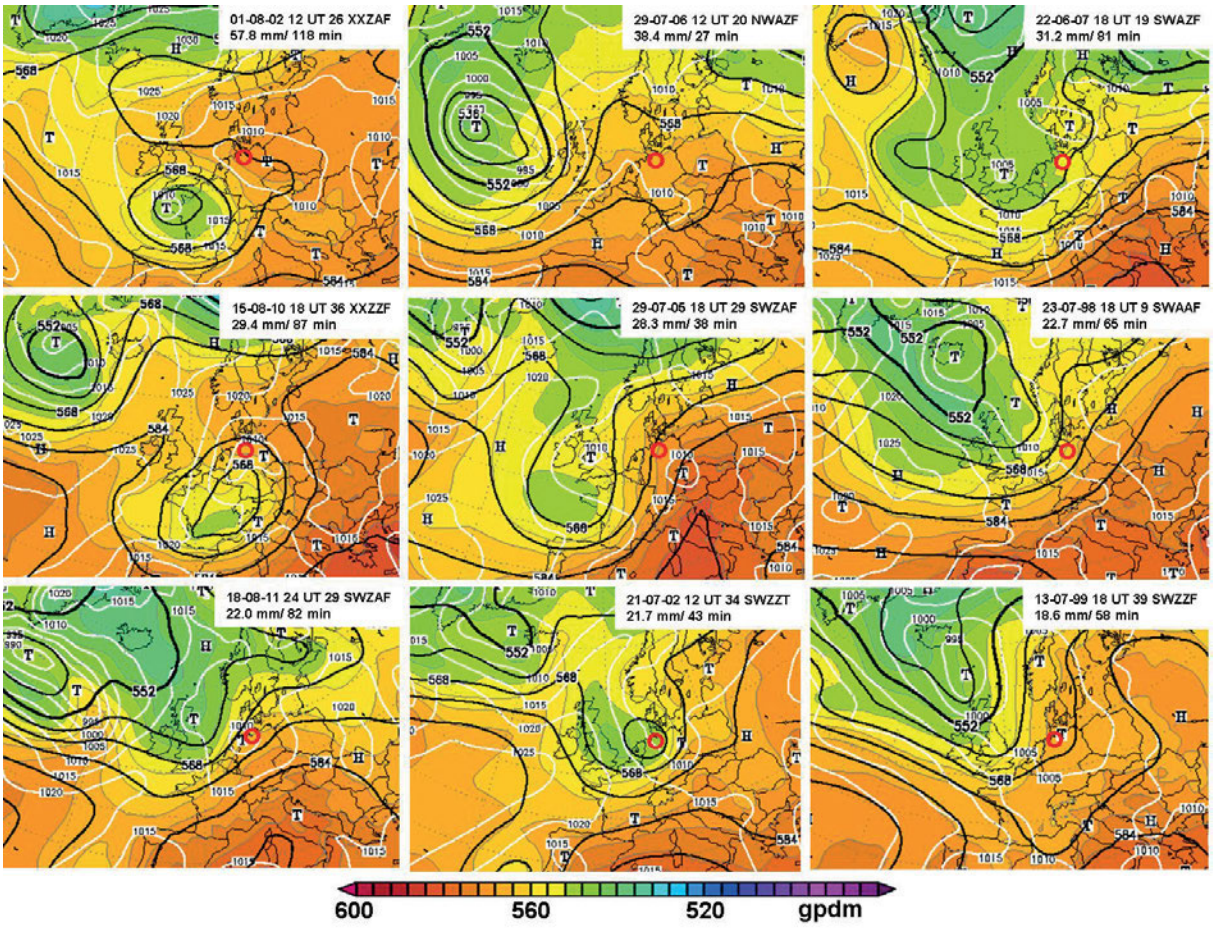

Figure 15: As Fig. 13, but for the nine most extreme summer-convective precipitation events.

convective situation in which convective cells could be embedded. If this low moves to a position northeast of Hamburg as mentioned above as a condition for extreme summer-stratifom cases, an extreme summer-convective situation may be followed by an extreme summer-stratiform situation. Such a synoptic situation in which strong convective and long-lasting rain can occur in combination has the potential of producing high extreme precipitation amounts. During the 17-year observation period it occurred six times that extreme daily summer events followed day after day (however not all cases as convective/stratiform combination). The highest 2-day sum was 80.7 mm (included in Fig. 5).

5 Summary and conclusions

Data of precipitation amount and duration measured at the Hamburg Weather Mast with 1-minute time resolution during a period of up to 17 years are used for a statistical analysis of precipitation for various aggregation times from minute to month. The statistics include mean values and PDFs, but primarily concentrates on extreme values which are defined here by the 95th, 99th percentile of the PDF and the absolute maximum. These three extremes are calculated for the total 17-year period and data subsets such as same months of the year and same hours of the day. This allows determining the annual cycle and diurnal cycle of extreme precipitation for various aggregation times.

The mean value of monthly precipitation amount has a distinct annual cycle with the maximum in July/August and the minimum in April. The mean value of precipitation duration has the maximum in December/January and the minimum in April. Thus, April is the driest month in both respects. Extremes of precipitation amount have their maxima in July/August and their minima in February. This holds for the extremes of the monthly data subsets as well as for the monthly exceeding frequencies of the 17-year extreme values and is valid for all aggregation times AT = 1d, 1 h, 1 min. The annual cycle comes out particularly clear for the short ATs of 1 h and 1 min and underlines the annual cycle of convective processes contributing to the generation of precipitation.

In the winter season, there is no strong diurnal cycle of precipitation extremes for AT = 1 h and 1 min. In contrast to that, a distinct diurnal cycle of extreme precipitation is present in the summer season. This holds for the hourly 99th percentile and absolute maximum as well as for the hourly exceedances of the overall 99th percentile

value (5.2 mm/h). The corresponding maxima all occur in the afternoon time window 14–18 CET. A similar diurnal cycle was found by Blenkinsop et al. (2016) for the summer season in the United Kingdom.

The 95th and 99th percentile values for the total 17-year period in the range 1 min < AT < 1 month are well represented by power laws with exponents of 0.61 and 0.55, respectively. This does not hold for the absolute maximum which is usually described by the Jennings (1950) power law with the exponent of 0.50 (e.g. Zhang et al., 2013). The Jennings law underestimates the extreme values particularly in the range AT < 1 h, i.e. in the time scale of heavy convection causing flash flooding. The deviation from the power law is also emphasized by the maximum/95th percentile ratio which increases from values around 2 for AT = 5 d–30 d to values above 20 for AT < 1 h. The ratio is largest for AT = 5–10 min in an aggregation time range where both strong 1-min precipitation intensity and duration of such strong intensities contribute to the exceptional deviation from the power law. Our findings in Fig. 5 could be of practical use in two respects: (a) to estimate the 95th and 99th percentiles for AT < 1d for those locations where only daily AT records are available and (b) to estimate absolute maxima for AT < 1d from the maximum/95th percentile ratio.

Extreme precipitation needs favourable synoptic conditions. We used the daily DWD weather-type classification to assess its applicability as downscaling predictor of extreme precipitation. The classification is based on 4 indices: wind direction at 700 hPa, cyclonality at 950 hPa and 500 hPa, and vertically integrated humidity. Extreme daily precipitation (> 13.8 mm/d) occurred with 22 of the 40 DWD weather types. All weather types with easterly wind directions are excluded. The probability that extreme precipitation occurs, when one of these 22 weather types occurs, is < 16 %.

The 28 extreme daily winter cases are distributed over 10 weather types. However, 3 of these types cover 71 % of all winter extremes. Weather type 10 (NWAAF) stands out with almost 40 %. In summer, the 58 extreme cases are distributed over 12 weather types. Again, some weather types dominate but more weather types than in winter. Four SW-weather types cover 57 % of all summer cases. Weather types 29 (SWZAF) and 39 (SWZZF) dominate with 19 and 17 %, respectively.

The wider range of weather types related with extreme precipitation in summer than in winter can be explained by the precipitation modes (stratiform, convective) involved. In winter, all 28 extreme cases are of stratiform nature. All cases are aligned around the 7 mm/h intensity line in the amount-duration diagram. In summer, only 1/3 of the 58 cases follow the same intensity line. A further third with > 15 mm/h can clearly be classified as convective nature. The last third is placed between both modes.

Composites of the 3 dominating weather types (stratiform-precipitation weather type 10 in winter, and convective-precipitation weather types 29, 39 in summer) calculated both for the extreme and non-extreme days hint at particular large-scale features during the extreme days. For weather type 10 with straight zonal jet over Hamburg it is an increased NW-SE pressure gradient at all levels indicating increased jet velocity and a more southerly origin of air mass indicating increased load of water vapour. The weather types 29 and 39 with SW flow ahead of an upper level trough show an increased cyclonality at the surface and increased jet velocity at upper level during the extreme days. In addition, type 39 shows increased upper-air cyclonality. Hence, upper air velocity, amount of vertically integrated humidity (instead of simple classification as dry and wet), and magnitude of low-level and upper-air cyclonality (instead of simple classification as positive and negative) have a potential to filter out extreme precipitation days.

The separate (stratiform, convective) inspection of the large-scale flow situations during the 9 most extreme winter and summer cases supports the conclusions drawn from the composites. Overarching features of the large-scale flow configuration which characterize extreme days but which are not covered by the four indices of the DWD classification have been identified. These features are in winter the presence of a strongly developed jet stream and in most cases a developing trough upstream of Hamburg (whose impact on Hamburg could be captured by assessing advection of positive vorticity) and in summer the position and strength of the upper-level trough. Summer extreme stratiform precipitation does not imply the same large-scale flow configuration as in winter. The winter stratiform weather type is a westerly strong-wind (jet stream) situation with an N-S temperature contrast. The summer stratiform weather type is a south-westerly trough situation with an E-W temperature contrast (warm air in the E). Additionally, summer stratiform extreme events are characterized by a surface low east of Hamburg. A low at this position leads to up-gliding of warm and moist air from E on top of cold North Sea air from NW. This emphasizes the importance of local factors in addition to the large-scale flow in generating extreme precipitation.

All in all, the applicability of DWD weather type classification as downscaling predictor for extreme precipitation reveals to be rather limited, because the DWD classification scheme shows low success in filtering out the above mentioned overarching features of the large-scale flow configuration. This limitation may be attributed to the coarseness of the DWD-classification parameters. Refined classification parameters adjusted to identify overarching features could improve the approach. However, in case of the outstanding weather types 10, 29, and 39 the DWD classification parameters show a considerable promising potential to serve as extreme-precipitation downscaling parameters because these weather types identify extreme-precipitation flow patterns connected with 40 % (type 10) of winter and 19 % (type 29) and 17 % (type 39) of summer extreme cases. Provided suitable refinement of classi-

fication parameters allows ruling out the non-extreme cases occurring under these weather-type conditions, up to 40 % of winter and 36 % of summer extreme-precipitation cases could be captured by those refined downscaling parameters.

Acknowledgements

We thank Michael Offermann and Ingo Lange from the Meteorological Institute of the University of Hamburg for the technical operation of the Hamburg Weather Mast facility and for the archiving and preparation of the data.This work was supported through the Cluster of Excellence 'CliSAP' (EXC177), Universität Hamburg, funded through the German Science Foundation (DFG).

References

Bauer, H.-S., T. Schwitalla, V. Wulfmeyer, A. Bakhshaii, U. Ehret, M. Neuper, O. Caumont, 2015: Quantitative precipitation estimation based on high-resolution numerical weather prediction and data assimilation with WRF – a performance test – Tellus A, **67**, 25047, DOI:10.3402/tellusa.v67.25047.

Berg, P., C. Moseley, J.O. Haerter, 2013: Strong increase in convective precipitation in response to higher temperatures. – Nature Geosci. **6**, 181–185.

Bissolli, P., E. Dittmann, 2001: The objective weather types classification of the German Weather Service and its possibility of application to environmental and meteorological investigations. – Meteorol. Z. **10**, 253–260.

Blenkinsop, S., E. Lewis, S.C. Chan, H.J. Fowler, 2016: Quality-control of an hourly rainfall data set and climatology of extremes for the UK, – Int. J. Climatol. **37**, 722–740, DOI: 10.1002/joc.4735.

Brümmer, B., I. Lange, H. Konow, 2012: Atmospheric boundary layer measurements at the 280 m high Hamburg weather mast 1995–2012: mean annual and diurnal cycles. – Meteorol. Z. **21**, 319–335.

Dierer, S., M. Arpagaus, A. Seifert, E. Avgoustoglou, R. Dumitrache, F. Grazzini, P. Mercogliano, M. Milelli, K. Starosta, 2009: Deficiencies in quantitative precipitation forecasts: sensitivity studies using the COSMO model. – Meteorol. Z. **18**, 631–645.

Dittmann, E., S. Barth, G. Müller-Westermeier, J. Lang, 1995: Objektive Wetterlagenklassifikation. – Ber. des Deutschen Wetterdienstes, Nr. **197**, Offenbach am Main.

Eggert, B., P. Berg, J.O. Haerter, D. Jacob, C. Moseley, 2015: Temporal and spatial scaling impacts on extreme precipitation. – Atmos. Chem. Phys. **15**, 5957–5971.

Fowler, H.J., S. Blenkinsop, C. Tebaldi, 2007: Linking climate change modelling to impact studies: recent advances in downscaling techniques for hydrological modelling. – Int. J. Climatol. **27**, 1547–1578.

Friedrichs, P., 2010: Statistical downscaling of extreme precipitation events using extreme value theory. – Extremes **13**, 109–132.

Gao, X., C.A. Schlosser, P. Xie, E. Monier, D. Entekhabi, 2013: An analogue approach to identify extreme precipitation events: evaluation and application to CIMIP5 climate models in the United States. – MIT Joint Program on the Science and Policy of Global Change, Report No. **253**, 33 pp.

Groisman, P., R. Knight, D. Easterling, T. Karl, G. Hegerl, V. Razuvaev, 2005: Trends in intense precipitation in the climate record. – J. Climate **18**, 1326–1350.

IPCC, 2007: Climate Change 2007: The physical science basis. – Fourth Assessment Report, Cambridge University Press.

Jennings, A.H., 1950: World's greatest observed point rainfalls. – Mon. Wea. Rev. **78**, 4–5.

Kanae, S., T. Oki, A. Kashida, 2004: Changes in hourly heavy precipitation at Tokyo from 1890 to 1999. – J. Meteor. Soc. Japan **82**, 241–247.

Kunkel, K.E., K. Andsager, D.R. Easterling, 1999: Long-term trends in extreme precipitation events over conterminous United States and Canada. – J. Climate **12**, 2515–2527.

Kurz, M., 1998: Synoptic Meteorology, – Training Guidelines of the German Meteorological Service No. **8**, Deutscher Wetterdienst.

Maraun, D., F. Wetterhall, A.M. Ireson, R.E. Chandler, E.J. Kendon, M. Widmann, S. Brienen, H.W. Rust, T. Sauter, M. Themessl, V.K.C. Venema, K.P. Chun, C.M. Goodess, R.G. Jones, C. Onof, M. Vrac, I. Thiele-Eich, 2010: Precipitation downscaling under climate change: recent developments to bridge the gap between models and the end user. – Rev. Geophys. **48**, RG3003/2010.

Müller, M., M. Kaspar, J. Matschullat, 2009: Heavy rains and extreme rainfall-runoff events in Central Europe from 1951 to 2002. – Nat. Hazards Earth Syst. Sci. **9**, 441–450.

O'Gorman, P.A., 2015: Precipitation extremes under climate change. – Curr. Cli. Change Rep. **1**, 49–59, DOI: 10.1007/s40641-015-0009-3.

Peralta-Hernandez, A.R., R.C. Balling, L.R. Barba-Martinez, 2009: Comparative analysis of indices of extreme rainfall events: Variation and trends from southern Mexico. – Atmosfera **22**, 219–228.

Perez-Zanon, N., M.C. Casas-Castillo, R. Rodriguez-Sola, J.C. Pena, A. Rius, J.G. Sole, A. Redano, 2016: Analysis of extreme rainfall in the Ebre Observatory (Spain). – Theor. Appl. Climatol. **124**, 935–944.

Sen Roy, S., M. Rouault, 2013: Spatial patterns of seasonal scale trends in extreme hourly precipitation in South Africa. – Appl. Geography **39**, 151–157.

Sukovich, E., M. Ralph, F. Barthold, D. Reynolds, D. Novak, 2014: Extreme quantitative precipitation forecast performance at the Weather Prediction Center from 2001 to 2011. – Wea. Forecast. **29**, 894–911.

Tammets, I., J. Jaagus, 2013: Climatology of precipitation extremes in Estonia using the method of moving precipitation totals. – Theor. Appl. Climatol. **111**, 623–639.

Van den Besselaar, E.J.M., A.M.G. Klein Tank, T.A. Buishand, 2012: Trends in European precipitation extremes over 1951–2010. – Int. J. Climatol. **33**, 2682–2689, DOI: 10.1002/joc.3619.

Westra, S., H.J. Fowler, J.P. Evans, L.V. Alexander, P. Berg, F. Johnson, E.J. Kendon, G. Lenderink, N.M. Roberts, 2014: Future changes to the intensity and frequency of short-duration extreme rainfall. – Rev. Geophys. **52**, 522–555, DOI:10.1002/2014RG000464.

Zhang, H., K. Fraedrich, X. Zhu, R. Blender, L. Zhang, 2013: World's greatest observed point rainfalls: Jennings (1950) scaling law. – J. Hydrometeorol. **14**, 1952–1957.

Zolina, O., C. Simmer, K. Belyaev, A. Kapala, S. Gulev, 2009: Improving estimates of heavy and extreme precipitation using daily records from European rain gauges. – J. Hydrometeorol. **10**, 701–716.